International Journal of Microwave and Wireless Technologies

cambridge.org/mrf

Quad-Band multi-polarized antenna with modified electric-inductive–capacitive resonator

Ghanshyam Singh[1,2], Binod Kumar Kanaujia[3], Vijay Kumar Pandey[4] and Sachin Kumar[5]

[1]Department of Electronics and Communication Engineering, Feroze Gandhi Institute of Engineering and Technology, Raebareli 229316, India; [2]Dr. A.P.J. Abdul Kalam Technical University, Lucknow 226031, India; [3]School of Computational and Integrative Sciences, Jawaharlal Nehru University, New Delhi 110067, India; [4]Department of Electronics and Communication Engineering, Noida Institute of Engineering and Technology, Greater Noida 201306, India and [5]School of Electronics Engineering, Kyungpook National University, Daegu 41566, Republic of Korea

Research Paper

Cite this article: Singh G, Kanaujia BK, Pandey VK, Kumar S (2022). Quad-Band multi-polarized antenna with modified electric-inductive–capacitive resonator. *International Journal of Microwave and Wireless Technologies* **14**, 65–76. https://doi.org/10.1017/S1759078721000106

Received: 17 September 2020
Revised: 13 January 2021
Accepted: 14 January 2021
First published online: 15 February 2021

Key words:
Circular polarization; compact antenna; ELC resonator; quad-band antenna

Author for correspondence:
Sachin Kumar,
E-mail: gupta.sachin0708@gmail.com

Abstract

A compact circularly polarized (CP) patch antenna is presented for modern communication systems. The prospective antenna consists of a microstrip-line inset-fed rectangular patch and a defected ground plane. A rotated rectangular slot and a modified electric-inductive-capacitive (m-ELC) resonator are introduced in the patch and the ground plane to achieve multiband behaviour. A corner of the radiating patch is truncated and an arrow-shaped stub is introduced for generating circular polarization. The physical area of the substrate is $0.26\lambda_0 \times 0.22\lambda_0$, and the radiator size is $0.16\lambda_0 \times 0.14\lambda_0$, where λ_0 is the free-space wavelength estimated at the lowest frequency. The measured ($S_{11} \leq$-10 dB) bandwidths of the antenna are 80 MHz (3.58%) at 2.23 GHz, 75 MHz (2.64%) at 2.84 GHz, 80 MHz (2.50%) at 3.19 GHz, and 70 MHz (1.82%) at 3.83 GHz. The measured 3-dB axial ratio bandwidths are 40 MHz (1.41%), 100 MHz (3.12%), and 60 MHz (1.57%) at 2.84, 3.20 and 3.82 GHz, respectively. The proposed planar antenna design does not need dual-feed or multi-layered patches for achieving multiple CP bands. It offers easy integration with the printed circuits of the communication systems.

Introduction

Multi-antennas are widely used in modern communication devices to improve performance of the wireless systems. As compared to the multi-antenna system, the multiband operation scale down the number of resonating elements, hardware complexity, design time, and overall cost. A multiband behaviour can be obtained by introducing slots on the radiator or ground surface. Recently, circularly polarized (CP) antennas received considerable attention from designers as they encounter multipath fading effects and polarization mismatch losses. In the literature, various CP antenna designs have been suggested for multiband function [1–24]. In [1], a dual-band CP antenna was developed with two imbricating patches. However, the alignment of the two patches is difficult in this antenna design. Dual-band stacked patch antennas with probe feed [2] and hybrid feed [3] were presented for circular polarization. But, the dual-band performance was achieved at the cost of design complexity. Single-layered dual-band CP antenna with concentric annular rings [4] and capacitively coupled annular-ring slot antenna [5] were reported. A patch antenna with a truncated corner was presented [6], where an arrow-shaped triangular stub was loaded on the patch for polarization agility. An L-shaped slot antenna was proposed with metasurface [7]. However, the extra layer changed the profile of the antenna.

A probe-fed dual-band CP antenna with four sequentially rotated shorted monopoles and a U-slot was presented [8]. Since the antenna employed vias, drilling is needed, therefore, it could be difficult to integrate on the printed circuit board (PCB). A dual-band dual-polarized antenna with D-shaped complementary split-ring resonator (CSRR) engraved on the ground surface was proposed [9]. A tapered microstrip line-fed hexagonal slot antenna was proposed with three L-shaped slits for wireless and satellite applications [10]. A trident-shaped dipole antenna was presented for 2.4/5.2/5.8 GHz WLAN applications [11], where the antenna was backed with high impedance surface (HIS). A triple-band CP antenna was proposed with two electromagnetically coupled radiating elements [12]. Planar triple-band CP monopole antenna designs with different slots were reported in [13, 14]. A tri-band monopole antenna was proposed with a Y-shaped radiator for WLAN and Wi-MAX [15]. The antennas were loaded with the split-ring resonator (SRR) for obtaining multiple CP bands [16–18]. A dual-band slot antenna was presented with extended corners and an array of inclined strips [19]. A

© The Author(s), 2021. Published by Cambridge University Press in association with the European Microwave Association

CAMBRIDGE UNIVERSITY PRESS

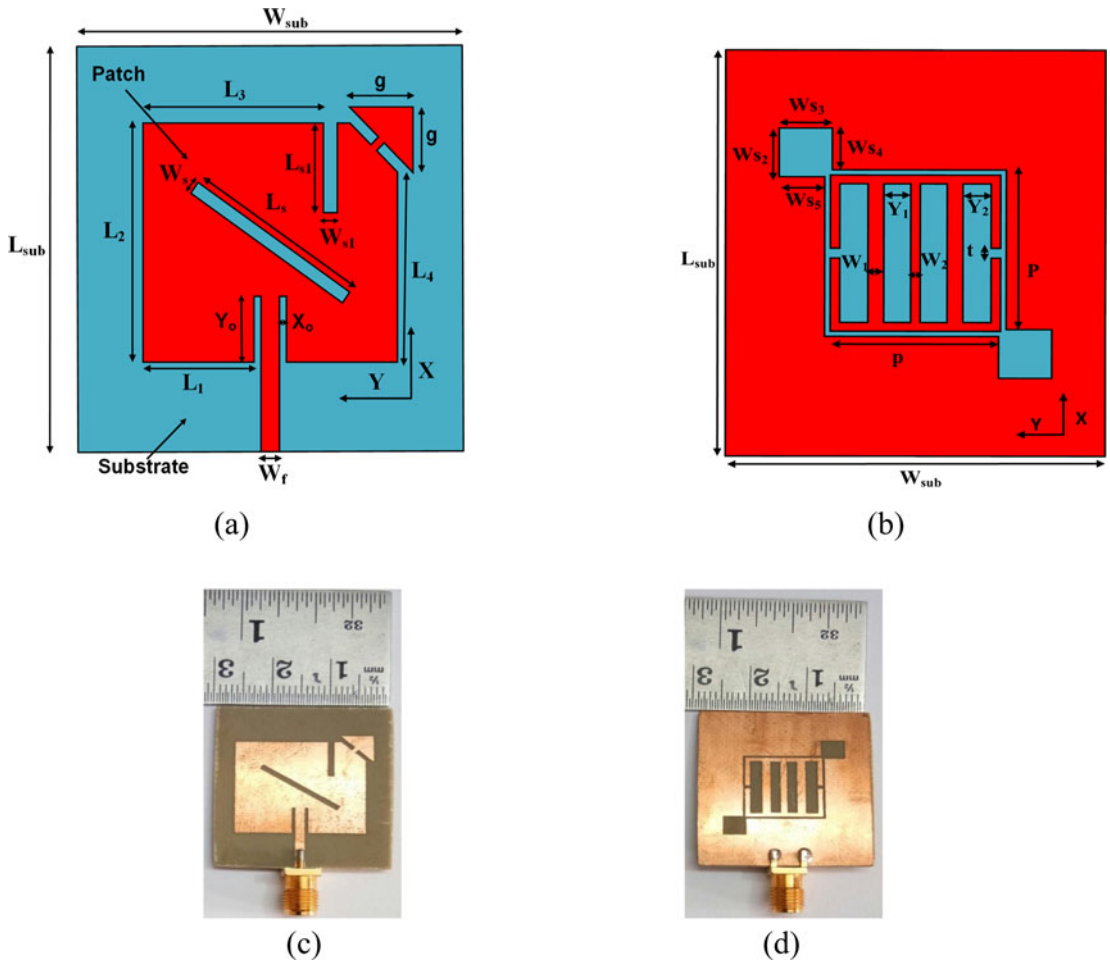


Fig. 1. Layout of the prospective CP antenna: (a) front view, (b) back view, (c) front view of the prototype, (d) back view of the prototype.

Table 1. Prospective antenna design parameters.

Parameter	W_{sub}	L_{sub}	L_1	L_2	L_3	L_4	L_S	W_S	L_{S1}	W_{S1}
Value (mm)	30	35	9.6	20	15.6	15.9	16	1.1	7.5	1.2
Parameter	W_{S2}	W_{S3}	W_{S4}	W_{S5}	W_1	W_2	W_f	g	t	Y_1
Value (mm)	4.2	4.2	3.6	3.6	1.25	0.75	3	5.5	0.85	2.125
Parameter	Y_2	P	p	h	α					
Value (mm)	2.225	13.75	13.45	1.6	55°					

coplanar waveguide (CPW)-fed broadband CP antenna was developed in [20], where rectangular, L-, and spiral slots were embedded in the antenna for circular polarization. A multi-polarized triple-band antenna was developed in [21], where asymmetric slots were loaded on the patch for achieving circular polarization. Dual-band single-layered antennas loaded with inverted L- and U-shaped strips were reported [22,23]. In [24], a 2 × 2 array of CP antenna elements was presented for IoT systems. However, the array used a complex sequential feeding mechanism. The antennas in [2, 3, 10, 11, 12] showed complex multi-layered geometry, therefore integration of such antennas into the PCB is difficult. The antenna sizes were relatively larger in [5, 8, 12,

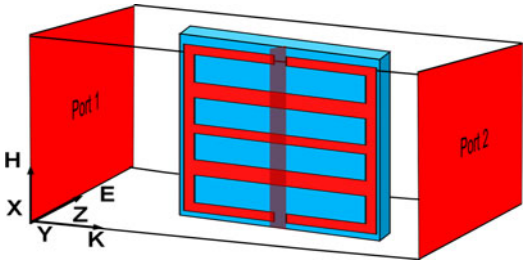


Fig. 2. Simulation set-up of an m-ELC resonator.

https://doi.org/10.1017/S1759078721000106 Published online by Cambridge University Press

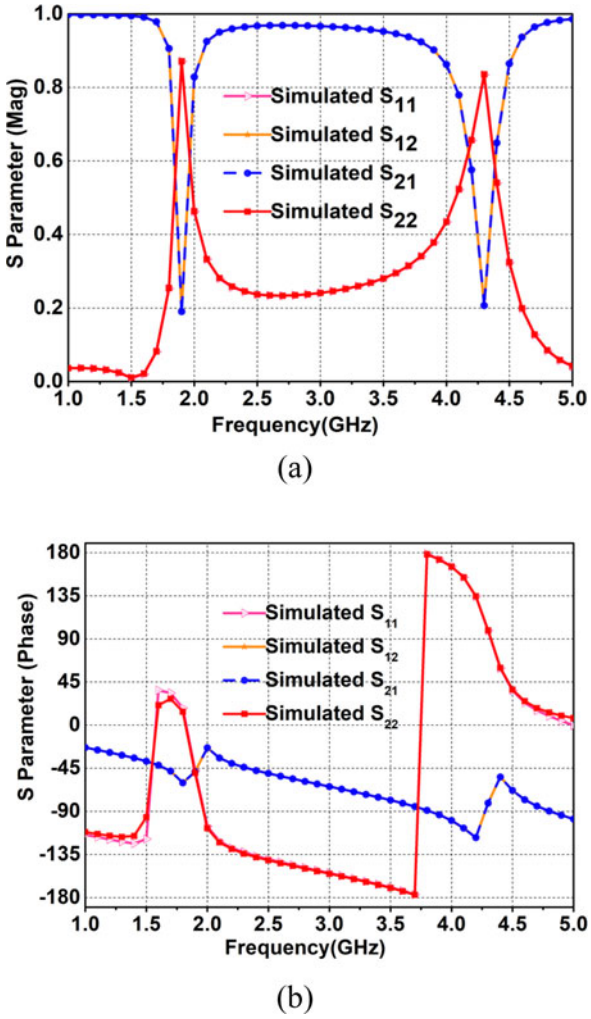


Fig. 3. Simulated outcomes of the prospective m-ELC (a) magnitude, (b) phase.

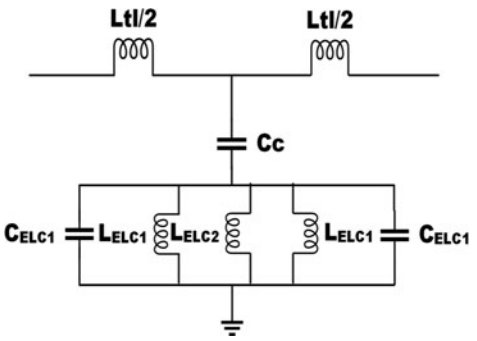


Fig. 4. Equivalent circuit of the proposed m-ELC.

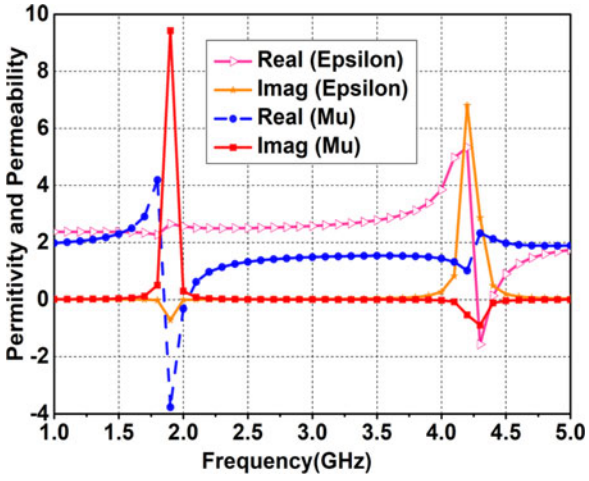


Fig. 5. Material parameters (ϵ_{m-ELC} and μ_{m-ELC}) of the prospective m-ELC.

15, 18, 20], therefore occupy more space, and this may also limit their integration with modern portable devices. The radiator designs in [19–21] were complex as they required an array of inclined strips and symmetric/asymmetric slots.

In this paper, a miniaturized, low-profile, single-feed multiband design composed of a microstrip-line inset-fed rectangular patch and a defected ground plane is presented. The multiband behaviour is obtained by introducing a modified electric–inductive–capacitive (m-ELC) resonator in the ground surface and a rotated rectangular groove in the patch. The antenna resonates

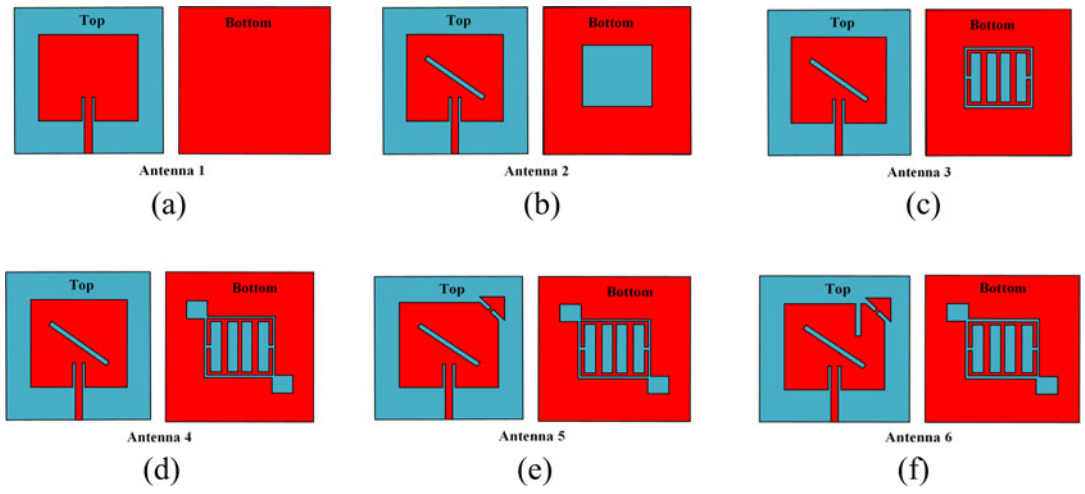


Fig. 6. Design steps of the prospective antenna.

https://doi.org/10.1017/S1759078721000106 Published online by Cambridge University Press

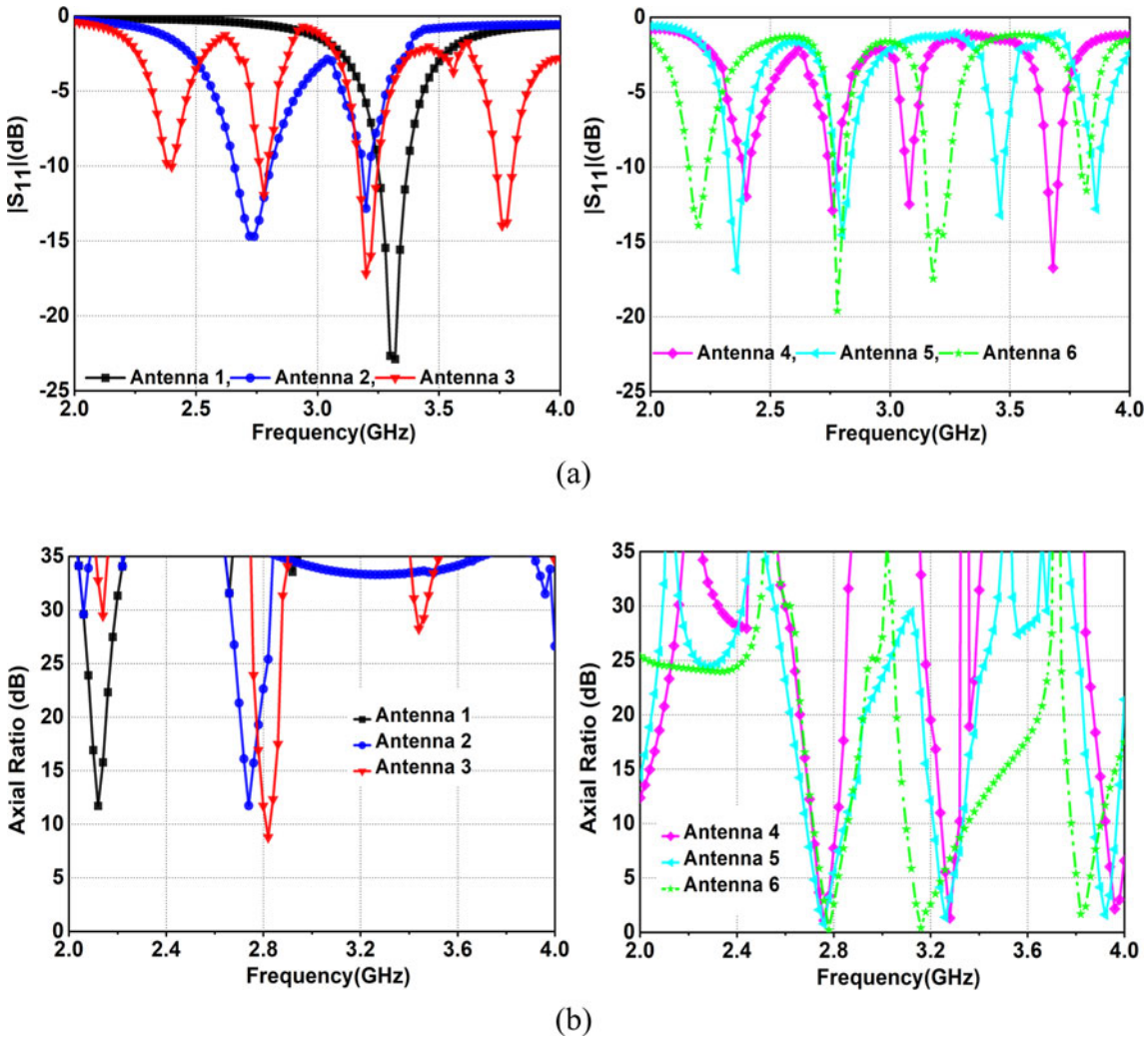


Fig. 7. Response of the design stages (a) S_{11}, (b) axial ratio.

at 2.2, 2.78, 3.18 and 3.82 GHz. For obtaining circular polarization, two square-shaped slots are engraved from the ground plane, and an arrow-shaped stub is introduced on the truncated patch of the antenna. Manufacturing of the prospective quad-band radiator is easy as it does not engage multiple feeds or special type of feeding method, vias, or stacked patches. The main contributions of the presented work are:

- The proposed antenna is a single-layered planar design, which offers easy integration with the PCB of the communication system.
- In the proposed multiband antenna, three CP bands are obtained without using a dual-feed or feeding network, therefore simplifying the antenna design procedure.
- The total area occupied by the prospective multiband antenna is comparatively small, and it can be easily integrated into portable RF devices.
- Most of the CP antenna designs reported in the open literature had the corner truncations for generating two orthogonal modes of the same magnitude and 90° phase difference, whereas the proposed design uses an arrow-shaped stub to achieve circular polarization.

Antenna configuration

The physical layout of the prospective antenna is demonstrated in Fig. 1. The presented CP planar antenna is simulated using

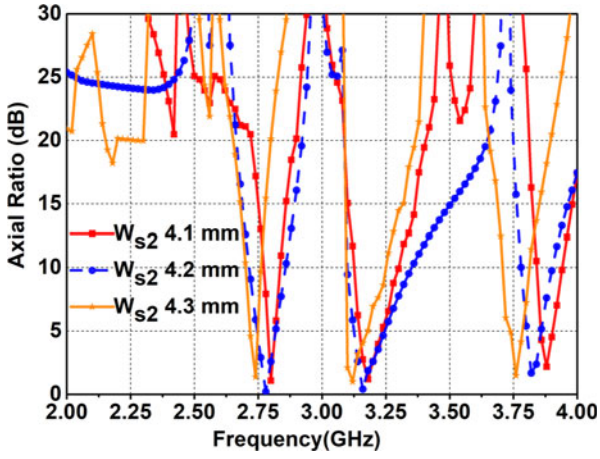
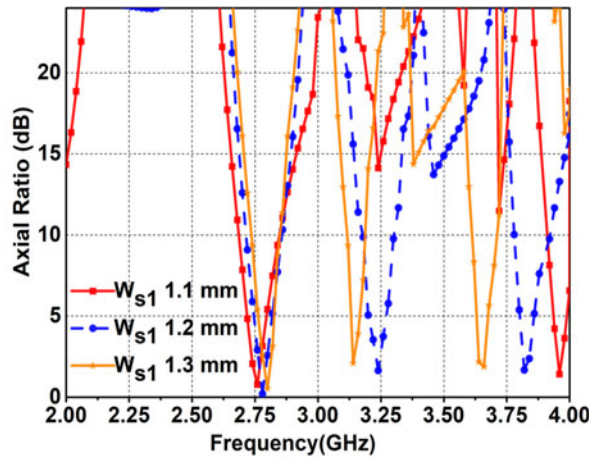
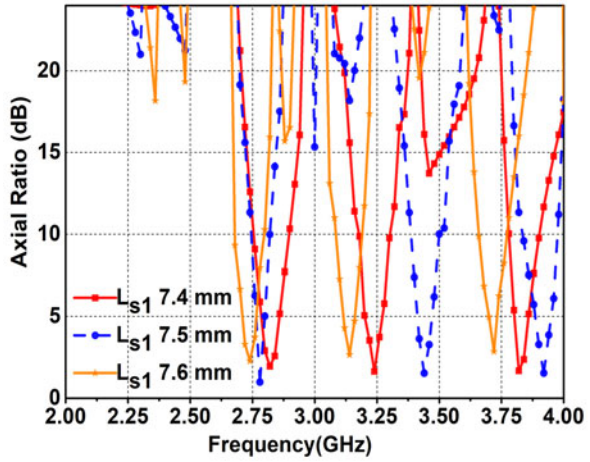


Fig. 8. Effect of Ws_2 on axial ratio.

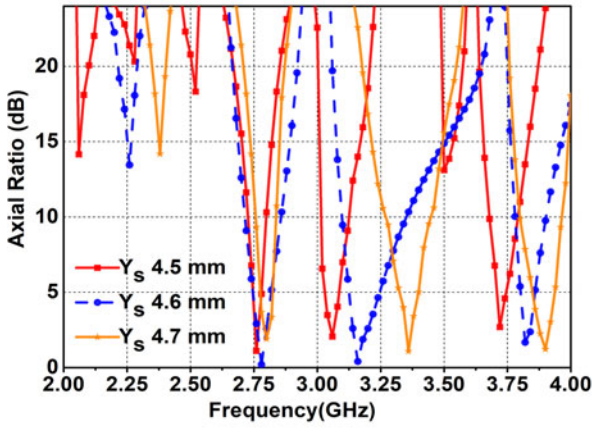
https://doi.org/10.1017/S1759078721000106 Published online by Cambridge University Press



(a)



(b)



(c)

Fig. 9. Effect of slit parameters on axial ratio (a) Ws_1, (b) Ls_1, (c) Ys.

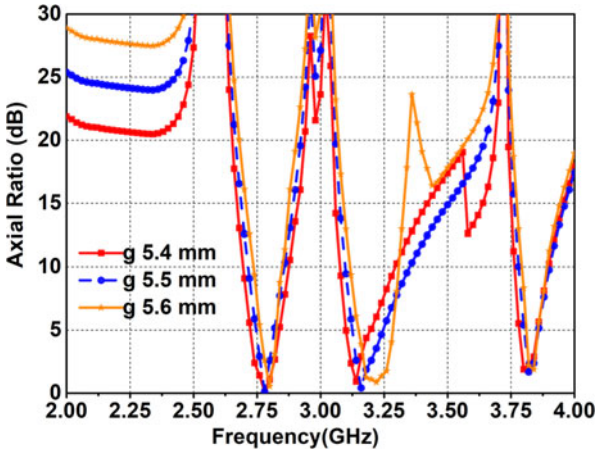
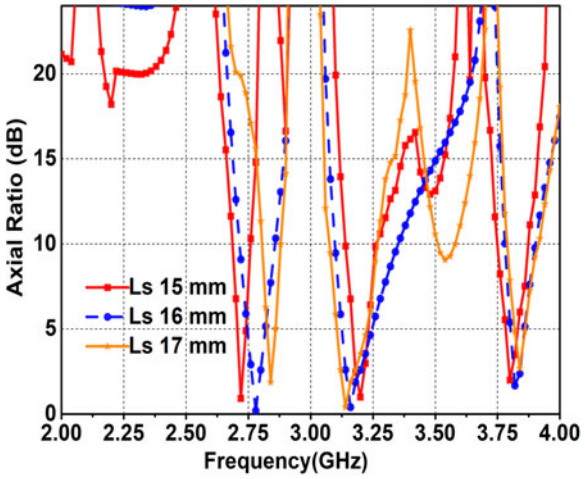
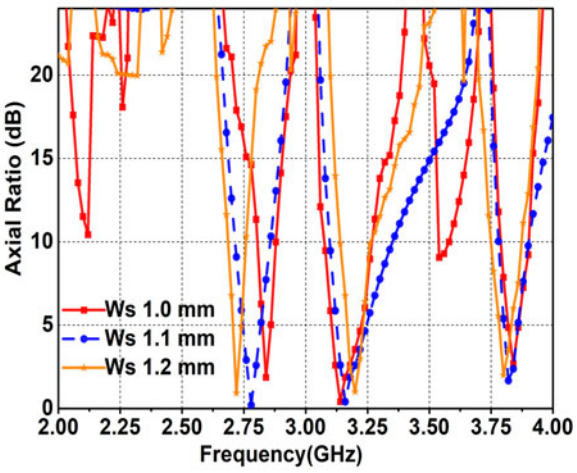


Fig. 10. Effect of arrow dimension (g) on axial ratio.



(a)



(b)

Fig. 11. Effect of diagonal slot parameters on axial ratio (a) Ls, (b) Ws.

ANSYS HFSS, and its prototype is printed on the FR-4 substrate (with relative permittivity (ε_r) of 4.4 and loss tangent (tan δ) of 0.02) of size $35 \times 30 \times 1.6$ mm^3. The physical parameters of the proposed antenna are presented in Table 1. The antenna consists of an inset-fed rectangular patch with truncated corner as shown in Fig. 1(a). The resonating patch is loaded with a rectangular slot for obtaining an additional resonance. A triangular-shaped stub is introduced at the corner of the patch for achieving circular

https://doi.org/10.1017/S1759078721000106 Published online by Cambridge University Press

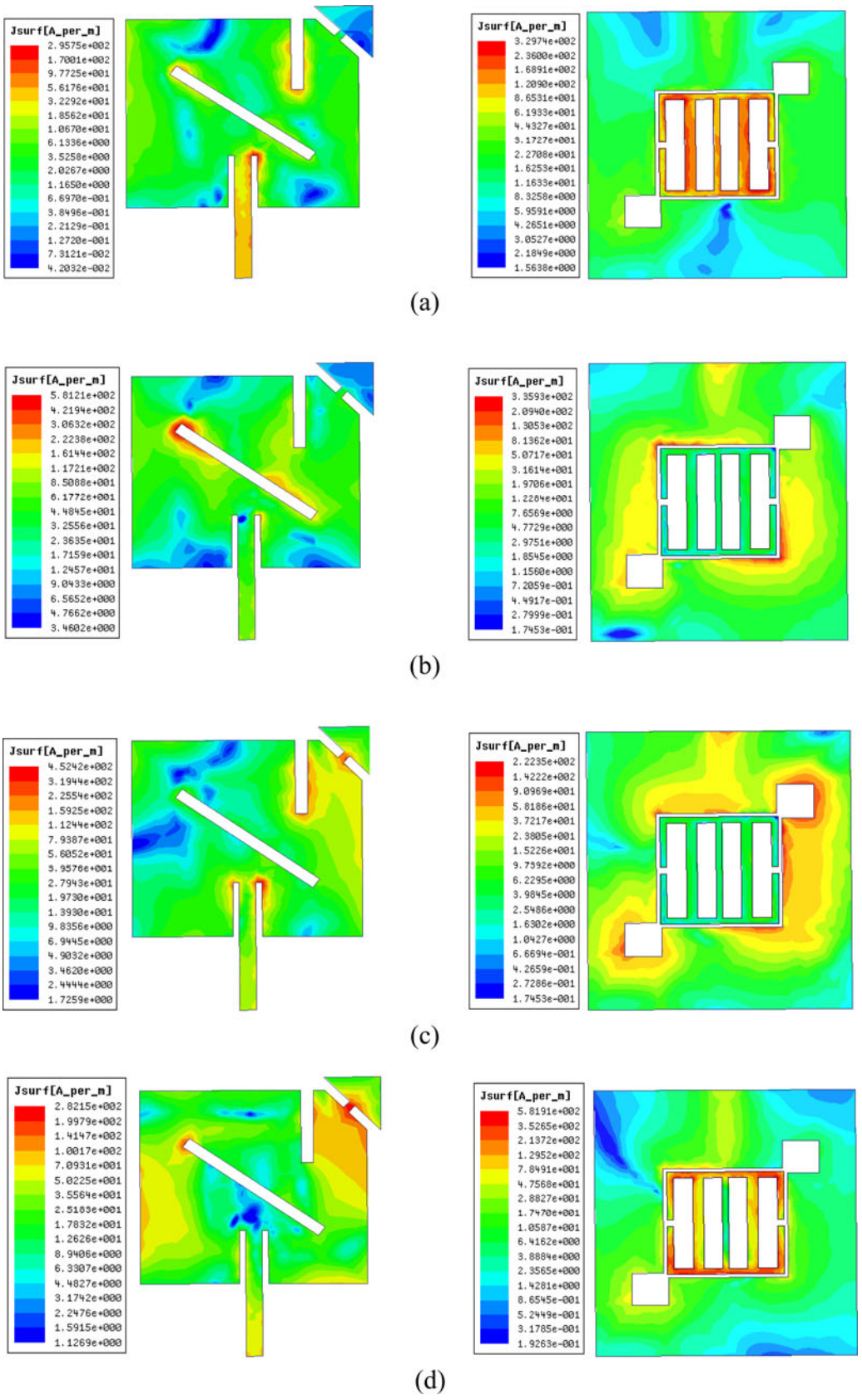


Fig. 12. Surface current circulation at different resonance frequencies (a) 2.2 GHz, (b) 2.78 GHz, (c) 3.18 GHz, (d) 3.82 GHz.

https://doi.org/10.1017/S1759078721000106 Published online by Cambridge University Press

polarization. Also, a rectangular slit is etched from the patch to shift the resonant band towards the lower frequency, thus decreasing the antenna size [25]. An m-ELC resonator and two square-shaped slots are engraved on the bottom side of the substrate for achieving CP multiband behaviour as shown in Fig. 1(b). The front view and back view of the fabricated prototype are portrayed in Figs 1(c) and 1(d), respectively.

Modified electric–inductive–capacitive (m-ELC) resonator

The physical parameters of the proposed m-ELC resonator are shown in Fig. 1(b). To analyze its operating behavior, the m-ELC resonator unit cell is simulated with a 50-Ω transmission line. The orientation and boundary conditions of the m-ELC unit cell are illustrated in Fig. 2. Figure 3 exhibits the reflection and transmission coefficients of the presented m-ELC.

In the simulation set-up, the feeding points are positioned along the *Y*-axis while the periodic boundaries (perfect electric conductor and perfect magnetic conductor) are positioned in the *Z*- and *X*-axes, respectively. A microstrip line is placed orthogonal to the feeding ports, and the input signal propagates from port-1 to port-2. The microstrip line responds to in-plane magnetic fields while the m-ELC resonator responds to orthogonal electric fields. Since m-ELC is working as a single negative metamaterial, the stop bands occur at 1.95 and 4.25 GHz, as illustrated in Fig. 3.

Furthermore, the prospective m-ELC resonator is studied with the help of circuit theory. In the past, various SRR/CSRR designs with 50-Ω microstrip line loading were investigated by many researchers [26–28]. The equivalent circuit of the prospective m-ELC is depicted in Fig. 4. Here, the m-ELC resonator is modeled as a parallel tank circuit while the microstrip line is modeled as an inductance L_{tl}. The coupling between the microstrip line and the parallel tank circuit is modeled as C_c. C_{ELC1} represents the capacitance of two outer rings, while L_{ELC1} and L_{ELC2} represent the inductance of outer and inner finger loops, respectively.

In the literature, several techniques have been reported to extract material parameters of the unit cell [29–33]. The parameters (ε and μ) of the proposed m-ELC are computed using Nicolson–Ross–Weir (NRW) method. Complex S_{11}, S_{12}, S_{21}, and S_{22} are used for computing (ε_{m-ELC} and μ_{m-ELC}) parameters. The refractive index (n_{m-ELC}) of m-ELC is calculated using the following bianisotropic medium formula [32].

$$n_{m-ELC} = \frac{1}{k.d_{m-ELC}} \cos^{-1}\left(\frac{1 - S_{11}S_{22} + S_{21}^2}{2S_{21}}\right) \quad (1)$$

It is evident that if $S_{11} = S_{22}$, then Eq. (1) will be the same standard retrieval equation given in [29]. During the computation of n_{m-ELC}, Eq. (1) has many possible solutions as discussed in references [29, 31]. For passive medium

$$\text{Im}\ (n_{m-ELC}) \geq 0 \quad (2)$$

In comparison to the isotropic medium, the bianisotropic medium has different characteristic impedance in different propagation directions (±*y* in the presented case).

$$z^+_{m-ELC} = \frac{\mu_{m-ELC}}{n_{m-ELC} + i\xi o} \text{ and } z^-_{m-ELC} = \frac{\mu_{m-ELC}}{n_{m-ELC} - i\xi o} \quad (3)$$

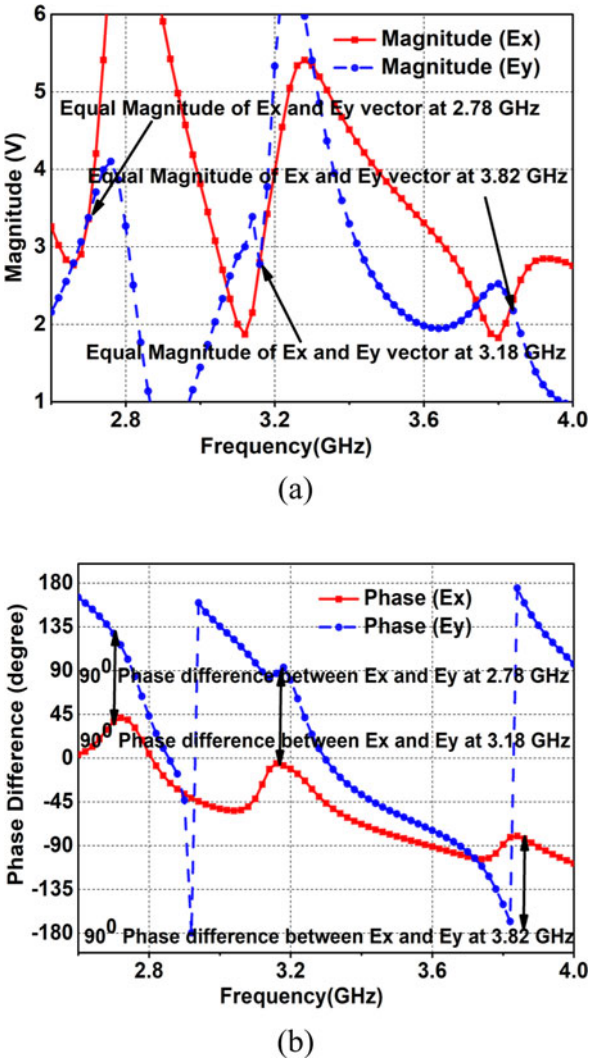


Fig. 13. Variations of E_x and E_y (a) magnitude, (b) phase.

$$\xi_0 = \left(\frac{n_{m-ELC}}{-2\sin(n_{m-ELC}.k.d_{m-ELC})}\right)\left(\frac{S_{11} - S_{22}}{S_{21}}\right) \quad (4)$$

$$\mu_{m-ELC} = \left(\frac{in_{m-ELC}}{\sin(n_{m-ELC}.k.d_{m-ELC})}\right) \times \left(\frac{2 + S_{11} + S_{22}}{2S_{21}} - \cos(n_{m-ELC}.k.d_{m-ELC})\right) \quad (5)$$

$$\varepsilon_{m-ELC} = \frac{(n^2_{m-ELC} + \xi_0^2)}{\mu_{m-ELC}} \quad (6)$$

For a passive medium, the impedances z^+_{m-ELC} and z^-_{m-ELC} must follow the given criteria

$$\text{Re}\,(z^+_{m-ELC}) \geq 0, \text{ and } \text{Re}\,(z^-_{m-ELC}) \geq 0 \quad (7)$$

where ξ_0 is the magneto-electric coupling coefficient, k is the free

https://doi.org/10.1017/S1759078721000106 Published online by Cambridge University Press

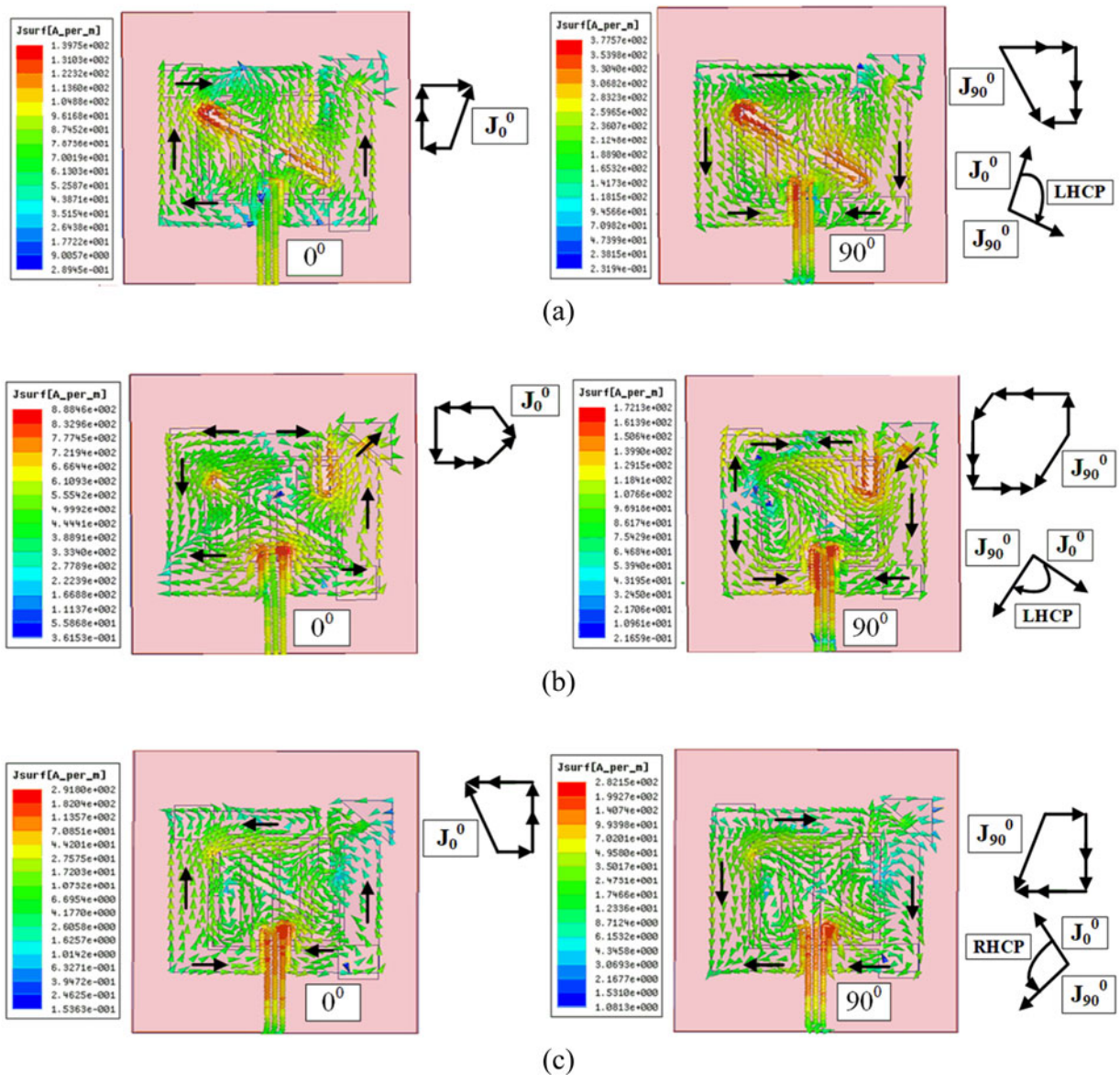


Fig. 14. Surface current circulation at (a) 2.78 GHz, (b) 3.18 GHz, (c) 3.82 GHz.

space wave number, and d_{m-ELC} is the largest dimension of the m-ELC unit cell.

The fundamental resonant frequency of an m-ELC is calculated as

$$\omega_0 = \sqrt{\frac{1}{L_{ELC}C_{ELC}}} \tag{8}$$

where L_{ELC} and C_{ELC} represent the total inductance and capacitance of the m-ELC, respectively. The parameters of the proposed m-ELC are plotted in Fig. 5, which shows negative metamaterial behavior at two resonant bands.

Development of the prospective antenna

The development stages of the prospective CP multiband antenna are demonstrated in Fig. 6. As shown in Fig. 6(a), the design process starts with Antenna-1, which is an inset-fed rectangular microstrip patch antenna operating at 3.35 GHz. The radiator size of the antenna-1 is 22×20 mm^2. The antenna is modified by introducing a wide slot and a rectangular slot (rotated by 55°) in the ground plane and the resonating patch, respectively, as demonstrated in Fig. 6(b). Antenna-2 exhibits dual-band linearly polarized attributes. As displayed in Fig. 6(c), the antenna-3 is realized by loading an m-ELC unit cell in the wide slot of the antenna-2.

In step 4, two square-shaped slots are etched from the ground of the antenna-3 as portrayed in Fig. 6(d). The square-shaped slots introduce a quadrature-phase difference between the two current vectors and also improve the impedance matching. Further, the rectangular patch is truncated and an arrow-shaped stub is introduced at the corner of the radiator to induce circular polarization (antenna-5) as illustrated in Fig. 6(e). In Fig. 6(f), a slit is cut along the top edge of the radiator for better impedance matching in the two upper bands. The return loss and axial ratio variations of the design steps are demonstrated in Figs 7(a) and 7(b), respectively.

https://doi.org/10.1017/S1759078721000106 Published online by Cambridge University Press

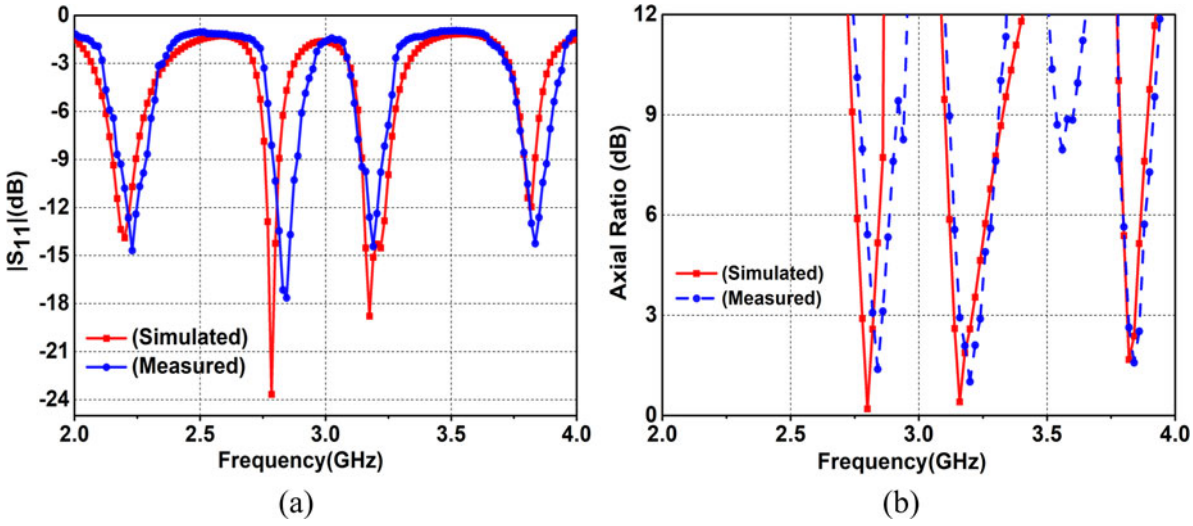


Fig. 15. Simulated and experimental outcomes (a) S_{11}, (b) axial ratio.

Parametric study of the prospective antenna

The parametric study of the prospective multiband CP antenna is demonstrated in Figs 8–11. The parametric analysis is divided into four stages. In stage 1, the effect of the ground plane slots (Ws_2, Ws_3) is studied. The values of Ws_2 and Ws_3 are varied and their effect on the axial ratio is observed. It is clear from Fig. 8 that Ws_2 affects the 3.8 GHz band significantly whereas a small influence is seen on the other bands. A similar effect is seen in the case of Ws_3.

In stage 2, the effect of slit dimensions (Ls_1, Ws_1, Ys) is presented in Fig. 9. The slit dimensions are optimized to shift 3-dB axial ratio bands at 3.18 and 3.82 GHz. The optimized dimensions of the slit are selected as $Ws_1 = 1.2$ mm, $Ls_1 = 7.5$ mm, and $Ys =$ 4.6 mm. In stage 3, the length (g) of the arrow-shaped patch is varied and its effect on the axial ratio band is presented. It is depicted in Fig. 10 that g influences the 3.18 GHz band significantly, and its value is chosen as 5.5 mm.

In stage 4, the effect of rectangular slot (Ls, Ws) is presented. It is depicted in Fig. 11 that Ls and Ws affect the 2.78 GHz band considerably, and their dimensions are chosen as 16 and 1.1 mm, respectively.

Results and analyses

The prospective antenna physical size is $0.26\lambda_0 \times 0.22\lambda_0$, and the radiator size is $0.16\lambda_0 \times 0.14\lambda_0$, where free-space wavelength (λ_0) is calculated at the first resonant frequency. In comparison to conventional antenna design, the loaded m-ELC saves space of ~62%. The quad-band resonances are obtained due to the slotted patch and m-ELC resonator. The etched slit/slot shifts resonant frequency towards the lower side, thus decreasing the size of the antenna [25]. The CP bands are obtained by means of the truncated corner, arrow-shaped stub, and square-shaped slots etched from the antenna ground.

The surface current circulation at 2.2, 2.78, 3.18 and 3.82 GHz is demonstrated in Fig. 12. It can be noticed in Fig. 12(a) that (at 2.2 GHz) the current concentration is high around the fingers of m-ELC. Whereas, at 2.78 GHz, the current concentration is high across the rectangular slot of the patch and wide slot of the ground, as demonstrated in Fig. 12(b). At 3.18 GHz, the current concentration is high around the square-shaped slots of the ground and slit of the patch as shown in Fig. 12(c). While, at 3.82 GHz, the current concentration is high around the periphery of the m-ELC resonator as displayed in Fig. 12(d).

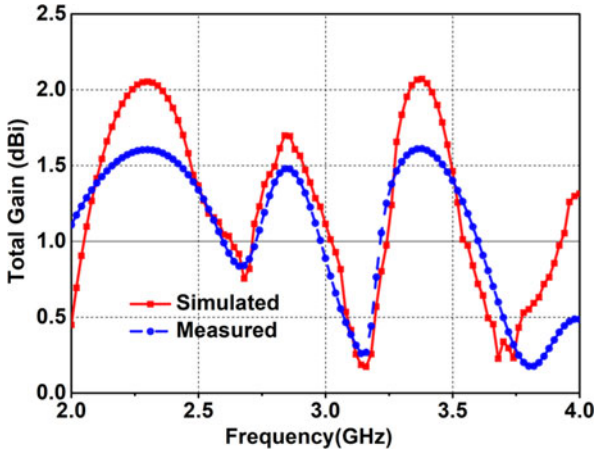


Fig. 16. Gain of the prospective antenna.

For obtaining circular polarization, the two electric field components (E_x and E_y) must have an equal magnitude ($|E_x| = |E_y|$) and quadrature-phase difference (±90°) between them. To get a better understanding of the polarization, the current vectors are examined at 2.78, 3.18 and 3.82 GHz. It is demonstrated in Fig. 13(a) that magnitude of the electric field components (in X-direction (E_x) and Y-direction (E_y)) is almost equal at 2.78, 3.18 and 3.82 GHz. The phase variation of two electric field components is illustrated in Fig. 13(b), which clearly illustrates that phase difference between the two fields is 90°.

To check the sense of polarization, the surface current vectors are plotted at 2.78, 3.18 and 3.82 GHz. It is clear from Fig. 14(a) that the resultant current vector rotates in a clockwise direction, which illustrates left-hand circularly polarized (LHCP) operation at 2.78 GHz. Similarly, at 3.18 GHz, the resultant current vector rotates in a clockwise direction, thus illustrating LHCP operation of the antenna, shown in Fig. 14(b). While, at 3.82 GHz, the

https://doi.org/10.1017/S1759078721000106 Published online by Cambridge University Press

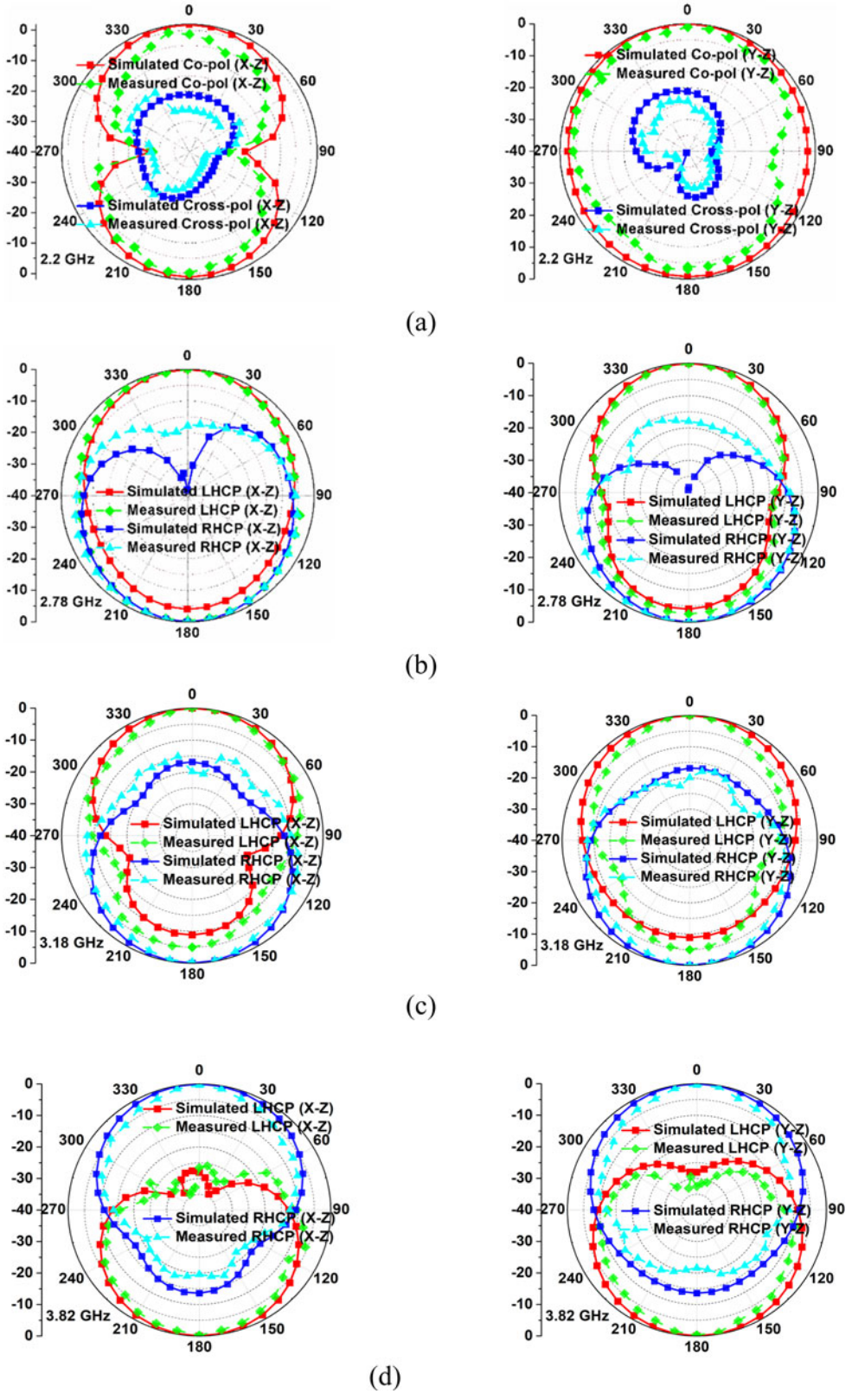


Fig. 17. Simulated and experimental patterns of the prospective antenna at (a) 2.2 GHz, (b) 2.78 GHz, (c) 3.18 GHz, (d) 3.82 GHz.

resultant current vector rotates in a counter-clockwise direction, thus illustrating right-hand circularly polarized (RHCP) operation of the antenna as illustrated in Fig. 14(b).

The experimental testing of the fabricated prototype is done using the Agilent N5230A PNA-L series vector network analyzer. Comparative outcomes of simulated and experimental return loss

https://doi.org/10.1017/S1759078721000106 Published online by Cambridge University Press

Table 2. Comparison of the prospective antenna with published multiband antennas.

Ref.	Bands (GHz)	Size of the antenna ($\lambda_0 \times \lambda_0$)	Peak gain (dB)	Impedance bandwidth (%)	Polarization
Prop.	2.23, 2.84, 3.19, 3.83	0.26 × 0.22	2.05, 1.3, 0.76, 0.3	3.58, 2.64, 2.50, 1.82	LP, CP, CP, CP
[5]	1.61, 2.74	0.35 × 0.30	2.5, 2.7	22.7, 22.3	CP, CP
[8]	1.575, 2.45	0.26 × 0.26	0.91, 6.8	0.7, 5.5	CP, CP
[12]	2.4, 3.5, 5.7	0.32 × 0.32	4.2, 5.5, 4	4.57, 3.37, 7.49	CP, CP, CP
[15]	2.4, 3.5, 5.8	0.36 × 0.28	2.3, 2.25, 0.6	9.16, 4.57, 66.37	CP, LP, CP
[18]	4.15, 4.77, 5.1	0.97 × 0.97	2.88, 1.96, 2.96	64.54	CP, CP, CP
[20]	6.99, 11.94	0.47 × 0.47	3.67, 6.36	92.70, 13.70	CP, CP
[21]	1.17645, 1.88, 2.3325	0.20 × 0.20	3, ---, 6.5	3.06, 4.36, 3.51	CP, LP, CP

are displayed in Fig. 15(a). The experimental −10 dB bandwidth is 80 MHz (3.58%) at 2.23 GHz, 75 MHz (2.64%) at 2.84 GHz, 80 MHz (2.50%) at 3.19 GHz, and 70 MHz (1.82%) at 3.83 GHz. The simulated impedance bandwidth is 90 MHz (4.09%) at 2.2 GHz, 70 MHz (2.51%) at 2.78 GHz, 100 MHz (3.14%) at 3.18 GHz, and 50 MHz (1.30%) at 3.82 GHz. The comparison between the simulated and measured axial ratio is illustrated in Fig. 15(b). The experimental 3-dB axial ratio bandwidths (in the +Z-direction) are 40 MHz (1.41%), 100 MHz (3.12%), and 60 MHz (1.57%) at 2.84, 3.20 and 3.82 GHz, respectively. Whereas, the simulated 3-dB axial ratio bandwidths are 60 MHz (2.15%), 80 MHz (2.51%), and 40 MHz (1.05%) at 2.78, 3.18 and 3.82 GHz. A small mismatch is seen between the simulated and experimental outcomes, which may be due to the fabrication and measurement errors. The comparison between simulated and measured gain is demonstrated in Fig. 16.

The radiation pattern measurements are conducted in a reverberation chamber with the help of an Agilent signal analyser (HP 8563E) and Anritsu (MG3694B) microwave signal generator. A standard horn antenna is used as a transmitter and the proposed antenna as a receiver. The physical separation (200 cm) between the transmitting and receiving antenna is fixed to satisfy the far-field conditions. The simulated and experimental patterns in E-(Y-Z) and H-(X-Z) planes are demonstrated in Fig. 17. It can be noticed in Fig. 17(a) that (at 2.2 GHz) bidirectional pattern is obtained in the E-plane, while in the H-plane, the pattern is omnidirectional. The antenna shows LHCP behavior (at 2.78 GHz and 3.18 GHz) in the E- and H-planes and RHCP behavior at 3.82 GHz as illustrated in Figs 17(b), 17(c), and 17(d).

A comparative study of the prospective design and other published CP multiband designs is conferred in Table 2. Most of the published multiband designs consisted of two/three layers, therefore, the alignment of multiple layers is an issue. The antenna reported in [8] consisted of four vias, therefore, it could be difficult to integrate on the PCB. In contrast to the previously published CP designs, the prospective design is low-profile, compact, and it does not need any external phase shifter or complex feed mechanism for introducing circular polarization. A low gain is realized, which is due to the modified ground plane of the antenna.

Conclusion

In this study, a compact low-profile quad-band antenna is suggested with three CP bands. The prospective inset-fed antenna comprised of a rectangular radiator and a modified ground surface. The multiband operation is achieved by loading an m-ELC resonator in the antenna ground and engraving a rectangular slot on the patch. The CP operation is achieved by truncating a corner of the patch and introducing an arrow-shaped stub in it. One more CP band is obtained by etching the opposite edges of the wide slot by means of two square-shaped slots. The prospective antenna is fabricated and measurement outcomes demonstrate a close affinity with the simulated results. The antenna operational frequency bands are 2.23, 2.84, 3.19, and 3.83 GHz. The prospective design is easy to manufacture, offers reasonable gain, and CP radiation at three bands. The antenna can be used for space to earth communication (2.17–2.2 GHz), airport surveillance radar/aviation services (typically operate in the 2.7–2.9 GHz range), Wi-MAX (3.3 GHz), and unmanned aerial vehicle (UAV)/Wi-MAX (3.8 GHz) applications.

References

1. **Beddeleem G, Ribero JM, Kossiavas G, Staraj R and Fond E** (2008) Dual-frequency circularly polarized antenna. *Microwave and Optical Technology Letters* **50**, 177–180.
2. **Nayeri P, Lee K-F, Elsherbeni AZ and Yang F** (2011) Dual-band circularly polarized antennas using stacked patches with asymmetric U-slots. *IEEE Antennas and Wireless Propagation Letters* **10**, 492–495.
3. **Yang J-S and Row J-S** (2017) Dual-band circularly polarized microstrip antenna. *Microwave and Optical Technology Letters* **59**, 404–408.
4. **Bao XL and Ammann MJ** (2007) Dual-frequency circularly-polarized patch antenna with compact size and small frequency ratio. *IEEE Transactions on Antennas and Propagation* **55**, 2104–2107.
5. **Wang C, Li J, Zhang A, Joines WT and Liu QH** (2017) Dual-band capacitively loaded annular-ring slot antenna for dual-sense circular polarization. *Journal of Electromagnetic Waves and Applications* **31**, 867–878.
6. **Pyo S and Shin I** (2012) A miniaturized switchable circularly polarized patch antenna controlled by a single diode operation. *Microwave and Optical Technology Letters* **54**, 2375–2378.
7. **Cao WQ, Zhang B, Hong W and Jin J** (2017) L-shaped slot coupling-fed low-profile broadband circularly polarized patch antenna with metasurface. *Journal of Electromagnetic Waves and Applications* **31**, 111–120.
8. **Wang MS, Zhu XQ, Guo YX and Wu W** (2018) Compact dual-band circularly polarised antenna with omnidirectional and unidirectional properties. *IET Microwaves, Antennas & Propagation* **12**, 259–264.
9. **Singh G, Kanaujia BK, Pandey VK, Gangwar D and Kumar S** (2019) Design of compact dual-band patch antenna loaded with D-shaped complementary split ring resonator. *Journal of Electromagnetic Waves and Applications* **33**, 2096–2111.
10. **Baek JG and Hwang KC** (2013) Triple-band unidirectional circularly polarized hexagonal slot antenna with multiple L-shaped slits. *IEEE Transactions on Antennas and Propagation* **61**, 4831–4835.
11. **Ta SX, Park I and Ziolkowski RW** (2013) Circularly polarized crossed dipole on an HIS for 2.4/5.2/5.8-GHz WLAN applications. *IEEE Antennas and Wireless Propagation Letters* **12**, 1464–1467.

https://doi.org/10.1017/S1759078721000106 Published online by Cambridge University Press

12. **Bao XL and Ammann MJ** (2014) Printed triple-band circularly polarized antenna for wireless systems. *Electronics Letters* **50**, 1664–1665.
13. **Xu R, Li J-Y, Q Y-X, Yang G-W and Yang J-J** (2017) A design of triple-wideband triple-sense circularly polarized square slot antenna. *IEEE Antennas and Wireless Propagation Letters* **16**, 1763–1766.
14. **Hoang TV and Chang Park HC** (2014) Very simple 2.45/3.5/5.8 GHz triple-band circularly polarised printed monopole antenna with bandwidth enhancement. *Electronics Letters* **50**, 1792–1793.
15. **Wu T, Shi X-W, Li P and Bai H** (2013) Tri-band microstrip-fed monopole antenna with dual-polarisation characteristics for WLAN and WiMAX applications. *Electronics Letters* **49**, 1597–1598.
16. **Kandasamy K, Majumder B, Mukherjee J and Ray KP** (2016) Dual-band circularly polarized split ring resonators loaded square slot antenna. *IEEE Transactions on Antennas and Propagation* **64**, 3640–3645.
17. **Paul PM, Kandasamy K and Sharawi MS** (2018) A tri-band circularly polarized strip and SRR loaded slot antenna. *IEEE Transactions on Antennas and Propagation* **66**, 5569–5573.
18. **Tharehalli Rajanna PK, Rudramuni K and Kandasamy K** (2019) Compact tri band circularly polarized planar slot antenna loaded with split ring resonators. *International Journal of RF and Microwave Computer-Aided Engineering* **29**, 1–9.
19. **Paul PM, Kandasamy K and Sharawi MS** (2020) A corner expanded slot antenna loaded with copper strips for dual-band circular polarization characteristics. *Microwave and Optical Technology Letters* **62**, 491–497.
20. **Jaiverdhan, Kumar A, Sharma M M and Yadav R P** (2019) Dual wideband circular polarized CPW-fed strip and slots loaded compact square slot antenna for wireless and satellite applications. *AEU – International Journal of Electronics and Communications* **108**, 181–188.
21. **Agrawal N, Gautam AK and Rambabu K** (2020) Design and packaging of multi-polarized triple-band antenna for automotive applications. *AEU – International Journal of Electronics and Communications* **113**, 152943.
22. **Weng WC, Sze JY and Chen CF** (2014) A dual-broadband circularly polarized slot antenna for WLAN applications. *IEEE Transactions on Antennas and Propagation* **62**, 2837–2841.
23. **Dardeer OM, Elsadek HA, Abdallah EA and Elhennawy HM** (2019) A dual band circularly polarized rectenna for RF energy harvesting applications. *Applied Computational Electromagnetics Society Journal* **34**, 1594–1600.
24. **Dardeer OMA, Elsadek HA and Abdallah EA** (2018) 2×2 Circularly polarized antenna array for RF energy harvesting in IoT system. *2018 IEEE Global Conference on Internet of Things (GCIoT), Alexandria*, Egypt. 1–6.
25. **Zachou V, Mayridis G, Christodoulou CG and Chryssomallis MT** (2004) Transmission line model design formula for microstrip antennas with slots. *IEEE Antennas and Propagation Society Symposium, 2004*, Monterey, CA, USA. 4, 3613–3616.
26. **Schurig D, Mock JJ and Smith DR** (2006) Electric-field-coupled resonators for negative permittivity metamaterials. *Applied Physics Letters* **88**, 041109.
27. **Baena JD, Bonache J, Martin F, Sillero RM, Falcone F, Lopetegi T, Laso MAG, Garcia JG, Gil I, Portillo MF and Sorolla M** (2005) Equivalent-circuit models for split-ring resonators and complementary split-ring resonators coupled to planar transmission lines. *IEEE Transactions on Microwave Theory and Techniques* **53**, 1451–1461.
28. **Gil I, Bonache J, Gil M, Garcia JG, Martin F and Marques R** (2006) Accurate circuit analysis of resonant-type left handed transmission lines with inter-resonator coupling. *Journal of Applied Physics* **100**, 074908.
29. **Smith DR, Schultz S, Markos P and Soukoulis CM** (2002) Determination of effective permittivity and permeability of metamaterials from reflection and transmission coefficients. *Physical Review B* **65**, 195104.
30. **Smith DR, Vier DC, Koschny TH and Soukoulis CM** (2005) Electromagnetic parameter retrieval from inhomogeneous metamaterials. *Physical Review E* **71**, 036617.
31. **Chen X, Grzegorczyk TM, Wu BI, Pacheco J Jr and Kong JA** (2004) Robust method to retrieve the constitutive effective parameters of metamaterials. *Physical Review E* **70**, 016608.
32. **Li Z, Aydin K and Ozbay E** (2009) Determination of the effective constitutive parameters of bianisotropic metamaterials from reflection and transmission coefficients. *Physical Review E* **79**, 026610.
33. **Chen L, Lei ZY, Yang R, Shi XW and Zhang J** (2013) Determining the effective electromagnetic parameters of bianisotropic metamaterials with periodic structures. *Progress in Electromagnetics Research M* **29**, 79–93.



Ghanshyam Singh received the B.Tech. degree in electronics and communication engineering from Uttar Pradesh Technical University, Lucknow, India, in 2004, and the M.E. degree in electronics and communication engineering from the National Institute of Technical Teachers Training and Research, Chandigarh, India, in 2013. In 2007, he joined the Department of Electronics and Communication Engineering, Feroze Gandhi Institute of Engineering and Technology, Raebareli, India, as a lecturer. He also worked as an electronics engineer in the Railway Testing Division of M/s Central Electronics Limited, India. Currently, he is working towards his Ph.D. degree in electronics engineering from Dr. A.P.J. Kalam Technical University, Lucknow, India. His research interests include patch antennas, artificial electromagnetic materials, and reconfigurable MIMO antennas.



Binod Kumar Kanaujia received the B.Tech. degree in electronics engineering from Kamla Nehru Institute of Technology, Sultanpur, India, in 1994, and the M.Tech. and Ph.D. degrees from the Department of Electronics Engineering, Indian Institute of Technology Banaras Hindu University, Varanasi, India, in 1998 and 2004, respectively. He is currently a professor with the School of Computational & Integrative Sciences, Jawaharlal Nehru University, New Delhi, India. He has been credited to publish more than 350 research articles with more than 2900 citations and h-index of 25 in several peer-reviewed journals and conferences. He had supervised 50 M.Tech. and 15 Ph.D. scholars in the field of RF and microwave engineering. He is currently on the editorial board of several international journals. He is also a member of several academic and professional bodies, such as the Institution of Engineers, India, the Indian Society for Technical Education, and the Institute of Electronics and Telecommunication Engineers of India. He had successfully executed five research projects sponsored by several agencies of the Government of India, such as DRDO, DST, AICTE, and ISRO.



Vijay Kumar Pandey received the B.E. degree in electronics engineering from the University of Poona, India, in 1990, and the M.E. degree in control and instrumentation from the University of Delhi, India, in 1997. He received the Ph.D. degree in electronics engineering from the Indian Institute of Technology Banaras Hindu University, Varanasi, India, in 2006. Currently, he is working as a professor in the Department of Electronics and Communication Engineering, Noida Institute of Engineering & Technology, Greater Noida, India. He received a grant of Rs. 14.5 lakhs under MODROB scheme from the All India Council for Technical Education, New Delhi, India, for establishing a project/research laboratory. His research interests include CP antennas, reconfigurable antennas, metamaterial-inspired antennas, and microwave components.



Sachin Kumar received the B.Tech. degree in electronics and communication engineering from Uttar Pradesh Technical University, Lucknow, India, in 2009, and the M.Tech. and Ph.D. degrees in electronics and communication engineering from Guru Gobind Singh Indraprastha University, Delhi, India, in 2011 and 2016, respectively. He is currently a researcher with the School of Electronics Engineering, Kyungpook National University, Daegu, South Korea. His current research interests include circularly-polarized antennas, reconfigurable antennas, ultra-wideband antennas, defected ground structure, and microwave components.

https://doi.org/10.1017/S1759078721000106 Published online by Cambridge University Press